High-charge and multiple-star vortex coronagraphy from stacked vector vortex phase masks

Artur Aleksanyan, Etienne Brasselet

High-charge and multiple-star vortex coronagraphy from stacked vector vortex phase masks

Artur Aleksanyan and Etienne Brasselet*

Univ. Bordeaux, CNRS, LOMA, UMR 5798, F-33400 Talence, France
**Corresponding author: etienne.brasselet@u-bordeaux.fr*

Optical vortex phase masks are now installed at many ground-based large telescopes for high-contrast astronomical imaging. To date, such instrumental advances have been restricted to the use of helical phase masks of the lowest even order, while future giant telescopes will require high-order masks. Here we propose a single-stage on-axis scheme to create high-order vortex coronagraphs based on second-order vortex phase masks. By extending our approach to an off-axis design, we also explore the implementation of multiple-star vortex coronagraphy. An experimental laboratory demonstration is reported and supported by numerical simulations. These results offer a practical roadmap to the development of future coronagraphic tools with enhanced performances.

OCIS codes: (070.6110) Spatial filtering; (050.4865) Optical vortices; (350.1260) Astronomical optics.

Understanding the formation, the evolution and surprising diversity of extrasolar planets is one of the major challenges of modern astrophysics. Since the early observations by Mayor and Queloz more than two decades ago [1], a few thousands of exoplanets have been detected [2]. Although the easiest way to get information about their surface or their atmosphere is the direct observation, only a few of them have been imaged directly. In practice, understanding the evolution of planetary systems and other faint astronomical objects, as well as the conditions of appearance of life other than on the earth thus depends on the development of high dynamic range imaging techniques. More specifically, the study of planets similar to those of the solar system is associated with two main difficulties: the high intensity contrast and the small angular separation between planets and their host stars. Coronagraphs are the instruments designed for such tasks. They allow selective suppression of the starlight to reveal the surrounding planets, if they lie at an angular separation larger than the inner working angle. The latter is usually defined as the angle where the flux of a planet is attenuated by 50% with respect to its far away value.

A particular kind of coronagraph — the vortex coronagraph — combines diffraction limited inner working angle, high throughput, and clear off axis discovery space. The concept was introduced more than 10 years ago [3,4] and consists of imparting a helical phase profile to the optical field in the Fourier plane of a telescope. Namely, the basic ingredient is a vortex phase mask ideally characterized with a pure phase transmission function $\tau_\ell(\phi) = \exp(i\ell\phi)$ for the light field, with ℓ being an even integer and ϕ being the polar angle in the transverse plane, which ensures that the diffraction of on axis incident light redistributes it outside the geometric image of the input pupil in the case of a circular aperture [5]. Therefore, the diffracted light can be totally suppressed by placing a diaphragm (so called Lyot stop) in the reimaged input pupil plane. Vortex coronagraphs have been found to be promising enough to foster long term design and manufacturing efforts to produce a helical phase mask of the second order ($\ell = 2$). Depending on the considered spectral range, a few technologies have been developed, e.g., (1) subwavelength gratings [3] today at work in several ground based large telescopes [6], (2) liquid crystal polymer masks [7] that have also been implemented on a few instruments [8,9], and (3) photonic crystals [10]. Future giant telescopes will require the management of pointing noise/errors, lower order aberrations, and finite spatial extension of the source, which implies the development of higher order vortex masks. Their realization is especially difficult for subwavelength gratings [6,11], while liquid crystal polymers allow easier fabrication of a vector vortex phase mask of the order higher than two [12].

Here we propose a solution to create high order vortex coronagraphs that can be readily implemented using already developed second order vortex coronagraphs, hence offering a practical solution for subwavelength gratings that fit well in the mid infrared domain. The idea relies on cascading N helical phase masks $\tau_{\pm 2}$ in order to get an effective helical phase mask $\tau_{\pm 2N}$. Then we extend this approach to an off axis design, enabling N star vortex coronagraphy in a simpler way and with better performances than the previous laboratory demonstration [13]. In both cases, we report on experimental and numerical investigations in the case of a double vortex mask ($N = 2$). The generalization to higher order situations is conceptually straightforward.

The experimental setup used to address the laboratory demonstration of our two propositions is depicted in Fig. 1(a). It consists of two point sources located at the infinity (aka "star 1" and "star 2") simulated by two laser beams with wavelengths

$\lambda = 633$ nm that propagate at an angle $\alpha_{1,2}$ from the axis of a telescope made by two identical plano convex lenses L_1 with focal length $f_1 = 100$ mm. A clear circular aperture of radius $R_1 = 1$ mm made of a metallic iris is placed in front of the first lens of the telescope and defines the input pupil plane. The latter is reimaged in the exit pupil plane located at a distance $2f_1$ from the second lens of the telescope, where a second iris with radius $R_2 = 0.75$ mm is placed and plays the role of the Lyot stop. Downstream, the setup allows us to switch between exit pupil imaging and source imaging according to a lens and a camera, as sketched in Figs. 1(b) and 1(c), respectively. Finally, the double vortex mask is placed in the Fourier plane of the telescope.

We use a double vortex mask prepared from two identical vectorial vortex masks ($VM_{1,2}$) made of a radially patterned liquid crystal polymer thin film acting as a half wave plate (HWP) whose optical axis orientation angle is given by $\psi = \phi$ [14]. The latter material structuring is illustrated by the four brush pattern observed between crossed linear polarizers; see Fig. 1(e). From a general point of view, considering plane waves and neglecting diffraction, such elements transform an arbitrary polarized incident field $\mathbf{E}_{\text{in}} = E_0(a\mathbf{c}_+ + b\mathbf{c}_-)$, where $\mathbf{c}_\pm = (\mathbf{x} \pm i\mathbf{y})/\sqrt{2}$ refers to the unit circular polarization basis in the (x, y) transverse plane, and (a, b) are constants; into the output field, $\mathbf{E}_{\text{out}} = E_0(a\mathbf{c}_- e^{2i\phi} + b\mathbf{c}_+ e^{-2i\phi})$ [15]. In other words, they behave as second order vortex masks with

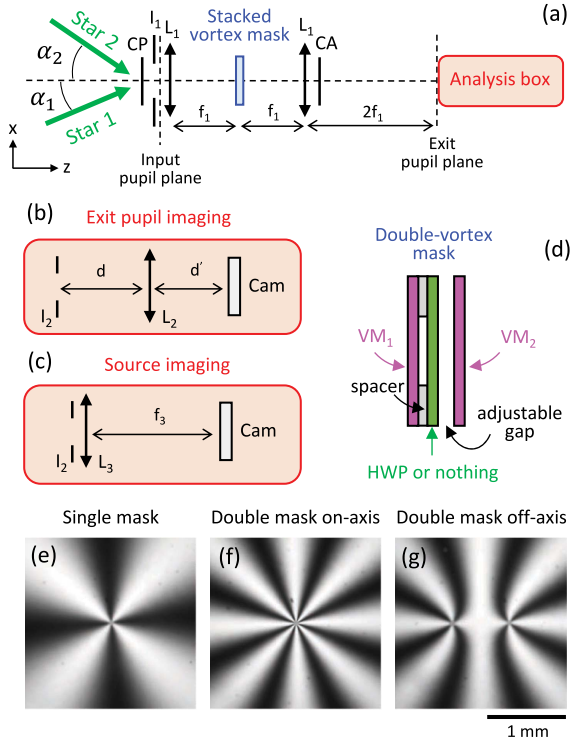

Fig. 1. (a) Setup. L_1, lens with focal length $f_1 = 100$ mm; I_1, iris with radius $R_1 = 1$ mm; CP/CA, circular polarizer/analyzer. (b) Exit pupil imaging. I_2, iris with radius $R_2 = 0.75$ mm; L_2, lens with $f_2 = 75$ mm; $1/d + 1/d' = 1/f_2$. (c) Source imaging. L_3, lens with $f_3 = 500$ mm; the camera is placed in the focal plane of L_3. (d) Sketch of the double vortex mask obtained by cascading two sec ond order vortex masks $VM_{1,2}$ and (or not) a HWP. (e), (f), (g) Crossed linear polarizer observations of single and double on/ off axis vortex masks.

transmission functions $\tau_{\pm 2}$ for the two orthogonal circular polarization states. Thus, by selecting an incident circular polarization and sandwiching a standard HWP between the two centered vortex masks, one gets the following field trans formation that does not depend on the HWP orientation up to an unimportant constant phase factor:

$$\mathbf{c}_\pm \xrightarrow{VM_1} \mathbf{c}_\mp e^{\pm 2i\phi} \xrightarrow{HWP} \mathbf{c}_\pm e^{\pm 2i\phi} \xrightarrow{VM_2} \mathbf{c}_\mp e^{\pm 4i\phi}. \quad \textbf{(1)}$$

Equation (1) emphasizes that the spin orbit arithmetic is a generic option to manipulate electromagnetic fields from geo metric phase optical elements [16]. This allows us to obtain a fourth order vortex mask with second order material structur ing. This is illustrated by the eight brush pattern observed between crossed linear polarizers; see Fig. 1(f). In practice, a 23 μm thick spacer is placed between the ∼100 μm thick HWP and VM_1 as depicted in Fig. 1(d), while VM_2 is ap proached near contact to HWP by a precision translation stage. The vortex masks are individually placed on a three dimensional translation stages enabling precise relative and absolute alignment. Circular polarizer/analyzer (CP/CA) are placed at the input/output of the telescope in order to get rid of residual VMs imperfections; see Fig. 1(a). In general, we note that the smaller the distance between VM_1 and VM_2, the better is the expected performance of the effective fourth order VM. In our case, the diffraction length associated with L_1 (>0.5 cm) is much larger than the VM interdistance which, therefore, is neglected when performing simulations.

Accordingly, the realization of a fourth order optical vortex coronagraph is demonstrated in Fig. 2 which displays the diffracted light pattern in the downstream pupil for single vortex [panel (a)] and double vortex [panel (b)] masks. Experimentally, this is done by using an on axis source ($\alpha_{1,2} = 0$) and imaging the exit pupil plane when the Lyot stop

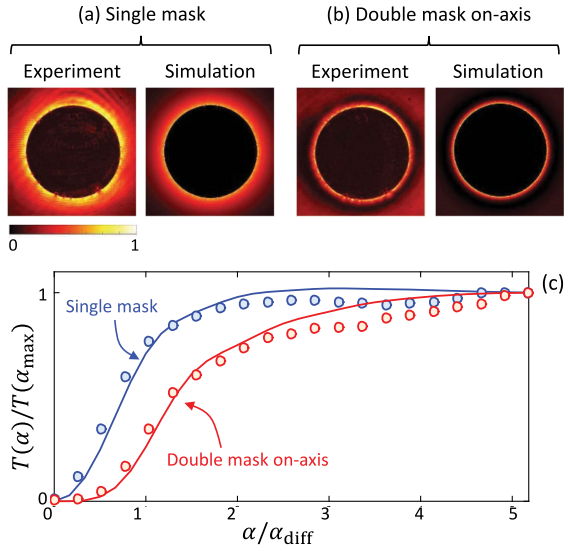

Fig. 2. Experimental and simulated redistribution of light of an on axis source outside the geometric image of the iris I_1 for (a) a single vortex mask and (b) a double vortex mask with HWP [here the Lyot stop is removed]. (c) Transmittance measured after the lens L_1 as a function of the normalized angular separation distance $\alpha/\alpha_{\text{diff}}$ to the telescope axis for single vortex (blue color) and double vortex (red color) masks. Markers, experimental data; solid curves, simulations. Transmittance is normalized to its value at $\alpha_{\max} = 5.18\alpha_{\text{diff}}$ in all cases.

is removed. The recorded images are compared with the analytical intensity patterns $I_\ell(r) = 0$ if $r < R_1$ and $I_\ell(r) = |(R_1/r)P^1_{|\ell|-1}(R_1/r)|^2$ otherwise where $P^1_{|\ell|-1}$ is the radial Zernike polynomial [17]. Quantitatively, the coronagraphic effect is evaluated by measuring the total power transmitted after the Lyot stop as a function of the angle α between the source propagation direction and the telescope axis; see Fig. 2(c) where $\alpha_{\text{diff}} = 0.61\lambda/R_1$ is the diffraction limit. Experimental data are compared with numerical simulations according to the expression of the transmittance through the Lyot stop, $T_\ell(\alpha) \propto \int_0^{2\pi}\int_0^{R_2} |\mathcal{F}^{-1}\{\tau_\ell(\phi)\mathcal{F}\{\text{circ}(r/R_1)\exp[ikr\sin\alpha]\}\}|^2 r\,dr\,d\phi$, where $k = 2\pi/\lambda$, $\mathcal{F}$ ($\mathcal{F}^{-1}$) refers to the (inverse) Fourier transform and $\text{circ}(r/R_1) = 1$ for $r < R_1$ and 0 otherwise. An obtained agreement validates the proposed single stage cascading approach.

Moreover, advanced coronagraphic functionality can be achieved by displacing the masks $\text{VM}_{1,2}$ from their initial position $(x, y) = (0, 0)$ to $(x_{1,2}, y_{1,2})$, which is done by translating the two vortex masks in the Fourier plane of the telescope. This is illustrated in Fig. 1(g) which displays a typical image of a double off axis vortex mask observed between crossed linear polarizers. In general, by considering the presence ($\Lambda = +1$) or not ($\Lambda = -1$) of the HWP, we obtain the field transformation

$$\mathbf{c}_\pm \xrightarrow{(\text{VM}_1+\text{HWP}) \text{ or } \text{VM}_1} \mathbf{c}_{\pm\Lambda}\frac{[(x-x_1)\pm i(y-y_1)]^2}{(x-x_1)^2+(y-y_1)^2}\cdots$$
$$\xrightarrow{\text{VM}_2}\mathbf{c}_{\mp\Lambda}\frac{[(x-x_1)\pm i(y-y_1)]^2}{(x-x_1)^2+(y-y_1)^2}\frac{[(x-x_2)\pm i\Lambda(y-y_2)]^2}{(x-x_2)^2+(y-y_2)^2}. \quad \textbf{(2)}$$

Following a previous work on the simultaneous eclipsing of multiple star systems by using independent localized second order laser induced vortex phase masks [13], the proposed double off axis vortex mask appears as an interesting upgrade since (1) there is no need to introduce a laser driving system inside the telescope, (2) an optimized solid state second order vortex mask can be used, and (3) the discovery space is no longer endowed with intrinsic dead zones. This is quantitatively investigated from numerical simulations in what follows.

First, we evaluate the coronagraphic performance of a double off axis mask toward the nulling of a mutually incoherent binary source separated by an angle $\alpha = \alpha_1 + \alpha_2$, taking $\alpha_1 = \alpha_2$ and centering $\text{VM}_{1,2}$ on star 1 and 2, respectively. Namely, assuming without loss of generality, that the propagation direction of the two sources lie in the (x, z) plane, we set $(x_{1,2}, y_{1,2}) = (\pm\alpha f_1/2, 0)$. Following Eq. (2), the corresponding transmission function expresses as

$$\tau(x, y; \alpha) = \frac{[(x-\alpha f_1/2)\pm iy]^2}{(x-\alpha f_1/2)^2+y^2}\frac{[(x+\alpha f_1/2)\pm i\Lambda y]^2}{(x+\alpha f_1/2)^2+y^2}, \quad \textbf{(3)}$$

where the $\pm$ sign refers to handedness of the incident circular polarization state, which has no influence on the obtained results. Quantitatively, we evaluate the joint binary power extinction ratio defined as the ratio between the power outside and inside the Lyot stop, $\mathcal{R}_{\text{power}}(\alpha) = \iint_{x^2+y^2>R_2^2} I(x, y; \alpha)\text{d}x\text{d}y / \iint_{x^2+y^2<R_2^2} I(x, y; \alpha)\text{d}x\text{d}y$ where $I = I_1 + I_2$ is the sum of the intensity profiles of the two sources (here chosen to be identical) in the exit pupil plane with $I_1(x, y; \alpha) = |\mathcal{F}^{-1}\{\tau(x, y; \alpha)\mathcal{F}\{\text{circ}(\sqrt{x^2+y^2}/R_1)\exp[ikx\sin(\alpha/2)]\}\}|^2$ and $I_2(x, y; \alpha) = I_1(x, y; -\alpha)$.

The results of simulations are shown in Fig. 3 for $\Lambda = \pm 1$, where the comparison with optimally located second order (thick blue curve) and fourth order (thick red curve) single vortex masks is also reported. The latter optimization refers to the fact that $\mathcal{R}_{\text{power}}$ depends both on the location of a single vortex mask and the angular separation of the binary sources: the best location for a single second order vortex mask is on axis [i.e., $(x, y) = (0, 0)$] for $\alpha/\alpha_{\text{diff}} \lesssim 1.39$ and centered on the Airy profile of one of the two sources [i.e., $(x, y) = (\pm\alpha f_1/2, 0)$] otherwise. A similar behavior is found in the case of a single fourth order vortex mask, but with a transition at $\alpha/\alpha_{\text{diff}} \simeq 2.40$. From these data, we conclude that a double mask with HWP always has a higher overall rejection than a single second order mask, while this remains true for a single fourth order mask only for $\alpha \gtrsim 1.32$. We note the necessary presence of HWP for $\alpha \lesssim \alpha_{\text{diff}}$, which can be qualitatively understood recalling that the effective mask tends to be uniform as $\alpha \to 0$ when $\Lambda = -1$, while it tends to a charge 4 vortex mask when $\Lambda = +1$ [see Figs. 3(b) and 3(c)]. In contrast, for $\alpha \gtrsim \alpha_{\text{diff}}$, the extinction is slightly better when the HWP is absent. Overall, the most robust situation refers to the case when HWP is present, which corresponds to present experimental investigations.

We also investigate the ability to reveal a faint source in the neighborhood of a binary star as a function of its angular position by evaluating the ratio $\eta = (I^{\max}_{\text{planet}}/I^{\max}_{\text{binary}})_{\text{ON}}/(I^{\max}_{\text{planet}}/I^{\max}_{\text{binary}})_{\text{OFF}}$ where $I^{\max}_{\text{planet}}$ refers to the peak intensity of a tertiary source (aka "planet"), $I^{\max}_{\text{binary}}$ refers to the peak intensity of the binary star system, and labels ON/OFF refer to situations when the binary star coronagraph is at work or not. Therefore, the larger the latter ratio, the better is the coronagraphic effect. The results are shown in Fig. 4 in the case of a planet with arbitrary location within the range $5 < \alpha_{x,y}/\alpha_{\text{diff}} < 5$ for two binary star systems characterized with $\alpha = 2\alpha_{\text{diff}}$ [Fig. 4(a)] and $\alpha = 5\alpha_{\text{diff}}$ [Fig. 4(b)]. Such maps emphasize one of the advantages of the single stage cascading approach versus the previous one based on laser induced

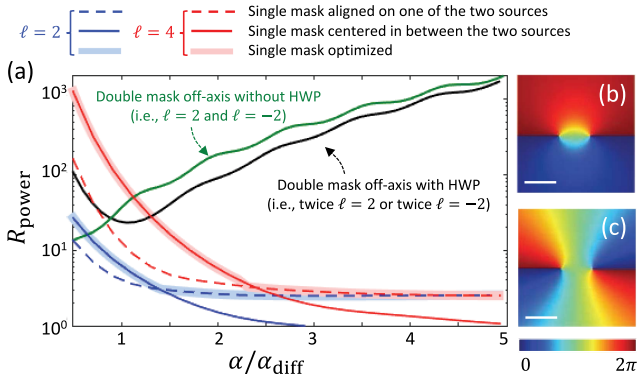

Fig. 3. (a) Calculated joint binary power extinction ratio for a binary source versus their angular separation α for different situations. Black/green curves: double off axis mask characterized by the transmission function given by Eq. (3) with $\Lambda = \pm 1$, respectively. Blue/red thin curves: situations where single second/fourth order vortex masks are placed either on one of the two sources or in between. Blue/red thick curves: optimized situation with respect to the latter case. (b), (c) Spatial profile of the effective phase mask without/with the HWP for $\alpha = \alpha_{\text{diff}}$. Scale bars: α_{diff}.

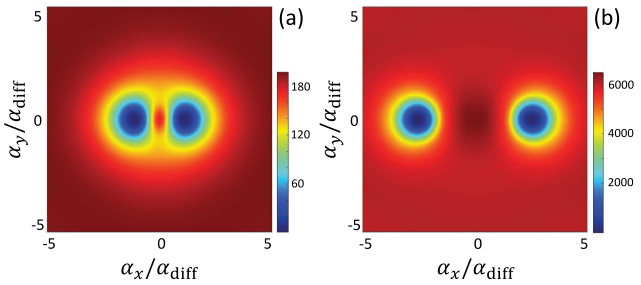

Fig. 4. Ratio η characterizing the ability to reveal a companion nearby a binary star (see in text definition) using a double off axis vortex mask for two binary star systems characterized with (a) $\alpha = 2\alpha_{\rm diff}$ and (b) $\alpha = 5\alpha_{\rm diff}$, where the angles $\alpha_{x,y}$ refer to angular directions in the (x, z) and (y, z) planes.

multiple vortex masks [13] regarding an enhanced discovery space without dead zones.

Finally, an experimental demonstration is made in the case of two binary star systems characterized with $\alpha = 2\alpha_{\rm diff}$ and $\alpha = 5\alpha_{\rm diff}$. In practice, we reimage the binary source in the presence of the Lyot stop when the double phase mask is at work or not, see Figs. 5(a) 5(d). In all cases, we also report on the corresponding simulations; see panels (e) and (f) in Fig. 5. Quantitatively, the recorded peak to peak intensity attenuation of the joint binary star when the coronagraph is activated is $\simeq$30 when $\alpha = 2\alpha_{\rm diff}$ and $\simeq$310 when $\alpha = 5\alpha_{\rm diff}$.

Summarizing, we have proposed and demonstrated a novel route to achieve (1) high charge optical vortex coronagraphy and (2) multiple optical vortex coronagraphy from a single stage strategy using spin orbit arithmetic associated with the cascade of several second order vortex phase masks. Importantly, the proposed approach does not require the development of higher order or inhomogeneous vortex phase masks. The practical consequence is that state of the art second order vortex phase masks already at work in large telescopes [6] could be combined to create and test high charge vortex coronagraphs. This implies the realization of HWPs having similar throughput and retardance performances

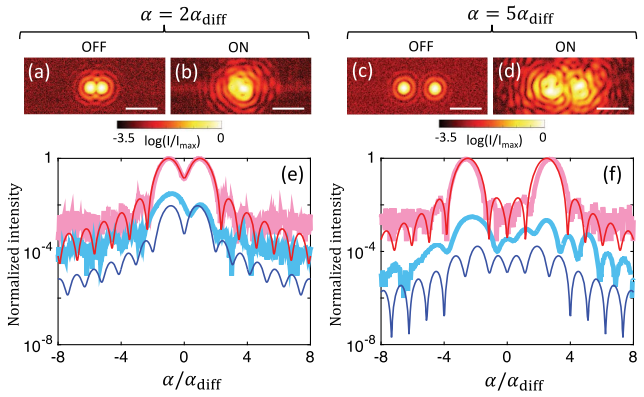

Fig. 5. Experimental reimaged binary sources when the binary star coronagraph is OFF and ON are shown in panels (a), (b) for a binary star system $\alpha = 2\alpha_{\rm diff}$ and in panels (c), (d) when $\alpha = 5\alpha_{\rm diff}$ with $I_{\rm max}$ being the maximal intensity of every image and where the logarithmic intensity range refers to the 4096 camera levels. Scale bars: $5\alpha_{\rm diff}$. (e), (f) Thick red/blue curves: raw intensity distributions along the binary star axis when the binary star coronagraph is OFF/ON. Thin red/blue curves: simulations.

which, however, does not represent a technological challenge. Moreover, the present scheme simplifies drastically the practical implementation of a multiple star vortex coronagraph. Recalling that a stellar multiplicity is a rather common event [18], the development of such a direct imaging tool is welcome. To date, a few proposals and attempts have been reported [19 23], but the assets of optical vortex coronagraphy are emerging only very recently in that context [13]. For this reason, the results in this Letter offer a practical roadmap to the realization of future coronagraphic tools with enhanced performances. Finally, we recall the need for achromatic solutions when developing vortex phase masks for coronagraphy, and we note that existing approaches for both subwavelength gratings [24] and liquid crystal polymer technologies [25] could be directly used when cascading low order phase masks.

Funding. Agence Nationale de la Recherche (ANR) (ANR 15 CE30 0018).

REFERENCES

1. M. Mayor and D. Queloz, Nature **378**, 355 (1995).
2. The Extrasolar Planets Encyclopaedia, http://exoplanet.eu/catalog/.
3. D. Mawet, P. Riaud, O. Absil, and J. Surdej, Astrophys. J. **633**, 1191 (2005).
4. G. Foo, D. M. Palacios, and G. A. Swartzlander, Opt. Lett. **30**, 3308 (2005).
5. G. A. Swartzlander, J. Opt. A **11**, 094022 (2009).
6. O. Absil, D. Mawet, M. Karlsson, B. Carlomagno, V. Christiaens, D. Defrère, C. Delacroix, B. F. Castella, P. Forsberg, J. Girard, C. A. G. González, S. Habraken, P. M. Hinz, E. Huby, A. Jolivet, K. Matthews, J. Milli, G. O. de Xivry, E. Pantin, P. Piron, M. Reggiani, G. J. Ruane, G. Serabyn, J. Surdej, K. R. W. Tristram, E. V. Catalán, O. Wertz, and P. Wizinowich, Proc. SPIE **9908**, 99080Q (2016).
7. D. Mawet, E. Serabyn, K. Liewer, C. Hanot, S. McEldowney, D. Shemo, and N. E. O'Brien, Opt. Express **17**, 1902 (2009).
8. E. Serabyn, D. Mawet, and R. Burruss, Nature **464**, 1018 (2010).
9. N. Jovanovic, F. Martinache, O. Guyon, C. Clergeon, G. Singh, T. Kudo, V. Garre, K. Newman, D. Doughty, J. Lozi, J. Males, Y. Minowa, Y. Hayano, N. Takato, J. Morino, J. Kuhn, E. Serabyn, B. Norris, P. Tuthill, G. Schworer, P. Stewart, L. Close, E. Huby, G. Perrin, S. Lacour, L. Gauchet, S. Vievard, N. Murakami, F. Oshiyama, N. Baba, T. Matsuo, J. Nishikawa, M. Tamura, O. Lai, F. Marchis, G. Duchene, T. Kotani, and J. Woillez, Publ. Astron. Soc. Pac. **127**, 890 (2015).
10. N. Murakami, S. Hamaguchi, M. Sakamoto, R. Fukumoto, A. Ise, K. Oka, N. Baba, and M. Tamura, Opt. Express **21**, 7400 (2013).
11. C. Delacroix, O. Absil, B. Carlomagno, P. Piron, P. Forsberg, M. Karlsson, D. Mawet, S. Habraken, and J. Surdej, Proc. SPIE **9147**, 91478Y (2014).
12. D. Mawet, J. T. Trauger, E. Serabyn, D. C. Moody, K. M. Liewer, J. E. Krist, D. M. Shemo, and N. A. O'Brien, Proc. SPIE **7440**, 74400X (2009).
13. A. Aleksanyan, N. Kravets, and E. Brasselet, Phys. Rev. Lett. **118**, 203902 (2017).
14. S. R. Nersisyan, N. V. Tabiryan, D. Mawet, and E. Serabyn, Opt. Express **21**, 8205 (2013).
15. L. Marrucci, C. Manzo, and D. Paparo, Phys. Rev. Lett. **96**, 163905 (2006).
16. L. Marrucci, C. Manzo, and D. Paparo, Appl. Phys. Lett. **88**, 221102 (2006).
17. A. Carlotti, G. Ricort, and C. Aime, Astron. Astrophys. **504**, 663 (2009).
18. G. Duchêne and A. Kraus, Annu. Rev. Astron. Astrophys. **51**, 269 (2013).
19. J. Crepp, E. Serabyn, J. Carson, J. Ge, and I. Kravchenko, Astrophys. J. **715**, 1533 (2010).
20. E. Cady, M. McElwain, N. J. Kasdin, and C. Thalmann, Publ. Astron. Soc. Pac. **123**, 333 (2011).
21. S. Thomas, R. Belikov, and E. Bendek, Astrophys. J. **810**, 81 (2015).
22. K. Wagner, D. Apai, M. Kasper, K. Kratter, M. McClure, M. Robberto, and J. L. Beuzit, Science **353**, 673 (2016).
23. J. Kühn and P. Patapis, Proc. SPIE **9912**, 99122M (2016).
24. C. Delacroix, P. Forsberg, M. Karlsson, D. Mawet, O. Absil, C. Hanot, J. Surdej, and S. Habraken, Appl. Opt. **51**, 5897 (2012).
25. Y. Li, J. Kim, and M. J. Escuti, Proc. SPIE **8274**, 827415 (2012).